Stabilization of an iridium oxygen evolution catalyst by titanium oxides

Journal of Physics: Energy

PAPER

Stabilization of an iridium oxygen evolution catalyst by titanium oxides

Olga Kasian[1,2,3], **Tong Li**[4], **Andrea M Mingers**[2], **Kevin Schweinar**[2], **Alan Savan**[5], **Alfred Ludwig**[5] **and Karl Mayrhofer**[6,7]

[1] Helmholtz-Zentrum Berlin GmbH, Helmholtz Institut Erlangen-Nürnberg, Hahn-Meitner-Platz 1, 14109, Berlin, Germany
[2] Max-Planck-Institut für Eisenforschung GmbH, Max-Planck-Str. 1, 40237, Düsseldorf, Germany
[3] Department of Materials Science and Engineering, Friedrich-Alexander-Universität Erlangen-Nürnberg, 91058, Erlangen, Germany
[4] Institute for Materials, Ruhr-Universität Bochum, Bochum 44801, Germany
[5] Chair for Materials Discovery and Interfaces, Institute for Materials, Faculty of Mechanical Engineering, Ruhr-Universität Bochum, 44801, Bochum, Germany
[6] Helmholtz-Institute Erlangen-Nürnberg for Renewable Energy (IEK-11), Forschungszentrum Jülich GmbH, 91058, Erlangen, Germany
[7] Department of Chemical and Biological Engineering, Friedrich-Alexander-Universität Erlangen-Nürnberg, 91058, Erlangen, Germany

E-mail: olga.kasian@helmholtz-berlin.de

Keywords: oxygen evolution reaction, stability, Ir–Ti catalyst

Supplementary material for this article is available online

OPEN ACCESS

RECEIVED
13 May 2020

REVISED
1 September 2020

ACCEPTED FOR PUBLICATION
30 September 2020

PUBLISHED
31 March 2021

Abstract

The anodic oxygen evolution reaction (OER) has significant importance in many electrochemical technologies. In proton exchange membrane water electrolyzers it plays a pivotal role for electrochemical energy conversion, yet sluggish kinetics and the corrosive environment during operation still compel significant advances in electrode materials to enable a widespread application. Up-to-date Iridium is known as the best catalyst material for the OER in acidic media due to its relatively high activity and long-term stability. However, scarcity of iridium drives the development of strategies for its efficient utilization. One promising way would be the formation of mixtures in which the noble catalyst element is dispersed in the non-noble matrix of more stable metals or metal oxides. A promising valve metal oxide is TiO_x, yet the degree to which performance can be optimized by composition is still unresolved. Thus, using a scanning flow cell connected to an inductively coupled plasma mass spectrometer, we examined the activity and stability for the OER of an oxidized Ir–Ti thin film material library covering the composition range from 20–70 at.% of Ir. We find that regardless of the composition the rate of Ir dissolution is observed to be lower than that of thermally prepared IrO_2. Moreover, mixtures containing at least 50 at.% of Ir exhibit reactivity comparable to IrO_2. Their superior performance is discussed with complementary information obtained from atomic scale and electronic structure analysis using atom probe tomography and x-ray photoelectron spectroscopy. Overall, our data shows that Ir–Ti mixtures can be promising OER catalysts with both high activity and high stability.

1. Introduction

With increasing environmental concerns, sustainable energy sources are anticipated to eventually replace traditional fossil fuels. However, such transition demands the development of environmentally friendly solutions for energy conversion and storage, especially due to the intermittent nature of renewables. In this regard, the balance between power generated by renewables and energy demand for end-use can be achieved by using electrochemical water splitting to produce hydrogen as the energy storage medium [1–3]. Proton exchange membrane water electrolysis (PEMWE) is considered as one of the most promising technologies for this purpose [4]. However, the widespread application of PEMWE is limited mainly by high cost and low efficiency of the electrocatalyst materials [5]. Materials that catalyze water decomposition should provide

high reactivity and maintain stability throughout long-time operation. This is especially crucial in case of the anodic oxygen evolution reaction (OER), due to the extremely corrosive acidic environment and the high potential required to drive this reaction [6–8]. Only a few materials are able to meet the necessary requirements to simultaneously provide sufficient reactivity and durability in harsh oxidizing conditions [9, 10]. Typically those are oxides with metallic-type conductivity, among which only iridium oxides are currently used in acidic water electrolyzers [4, 11, 12]. Nevertheless, even Ir-based catalysts slowly undergo dissolution [13–17]. Considering the scarcity and high price of Ir, optimization of its utilization and suppression of degradation become of pivotal importance. Mixing of Ir with other more stable materials, e.g. Ti [18–22] or Sn [23–25] typically results in catalysts showing very high stability against dissolution, but leads to penalties in terms of reactivity. Electrocatalytic performance deteriorates because of the inactivity of the non-noble surface elements and the insulating nature of stoichiometric TiO_2 and SnO_2 [19–21]. Nevertheless, the idea of mixing Ti and Ir in an optimized ratio remains attractive for achieving a beneficial compromise between catalytic activity and stability at low noble metal loading. During the last decades, numerous research efforts have been focused on the electrochemical and surface properties of anodes based on such alloys or oxides, and the current utilization of TiO_2 [26–28] and SnO_2 [29, 30] as catalyst supports for Ir catalyst nanoparticles confirms the success of the approach. Particularly, Ir–Ti oxide systems can maintain good reactivity during long term operation [21, 31, 32], yet a systematic investigation of the dependence of the performance on Ir–Ti composition with identical morphologies and operation conditions is still missing. Moreover, the origin of the improved stability in such systems and the interplay between composition and activity-stability trends remains an open question.

Herein, OER reactivity and stability of model Ir–TiO_x thin film electrodes covering a wide composition range are evaluated in acidic media using an electrochemical scanning flow cell connected to an inductively coupled plasma mass spectrometer (SFC-ICP-MS). Identical experimental protocols are applied in order to obtain systematic and comparable information on electrocatalytic properties of these catalysts. It is found that materials containing 40–50 at.% of Ir exhibit reactivity comparable to thermally prepared IrO_2, with dissolution below the detection limit of the ICP-MS. The obtained results on activity and stability trends for the Ir–TiO_x electrodes are compared to Ir–Ru and Ir–Sn mixed oxides and discussed in light of their potential utilization in water electrolysers.

2. Experimental

The details on experimental setups and Ir–Ti thin-film material library characterization are shown in the supplementary information (SI, figure S1–S3 (available online at stacks.iop.org/JPENERGY/3/034006/mmedia)). In short, the material libraries of Ir–Ti alloys were prepared by combinatorial-magnetron sputtering (DCA Instruments, Turku, Finland) employing a con-focal co-deposition approach (figure S1). Single crystal Si wafers (100) with a 1.5 μm barrier layer of thermal SiO_2 were used as substrates. Using such smooth substrates allows preparation of samples with minimized surface roughness. The substrates were cleaned in acetone and then isopropanol in an ultrasonic bath and dried with compressed, dry air before loading to the deposition chamber. The base pressure in the main chamber prior to deposition did not exceed $2.7 \cdot 10^{-6}$ Pa. The 100 mm diameter targets of Ti (99.995%, FHR, Germany) and Ir (99.9%, Evochem, Germany) were precleaned by sputtering with closed shutters prior to deposition. Ar (99.999%) was used as the sputter gas and the pressure in the chamber was adjusted to 0.67 Pa at room temperature. A 20 nm Ti adhesion layer was deposited at 200 W RF with a constant substrate rotation of 20 rpm, in order to produce uniform layer thicknesses from the confocal cathode arrangement. Then Ir and Ti were deposited simultaneously at 79 W RF and 157 W RF, respectively. The total growth rate was 0.03 nm s^{-1}. Due to the confocal cathode arrangement and the cathode tilt with respect to the substrate surface, thickness gradients are produced (see figure S4) when the substrate is static. As a result, the composition ratio of the co-sputtered elements in the mixture is dependent on the position on the sample surface. The composition of the obtained libraries was confirmed using EDX mapping as shown in figure S3 (INCA X-act, Oxford Instruments, U.K.) and x-ray photoelectron spectroscopy (XPS). After deposition, the samples were thermally treated in air at 350 °C for 4 h. This procedure leads to the formation of a continuous composition spread of oxide films with different Ti and Ir contents. After the high-throughput characterization of the material library for desired properties, the most promising compositions were synthesized as individual samples.

XPS measurements were performed to ensure the composition of the material library after annealing (Quantera II, Physical Electronics, Chanhassen, MN, USA). A monochromatic Al KαX-ray source (1486.6 eV) was applied at 15 kV and 25 W. The binding energy scale was referenced to the C 1 s signal at 285.0 eV. Analysis of the spectra was carried out using the Casa XPS (http://www.casaxps.com/) software. The compositions of the electrodes are shown in Ir–Ti atomic ratios, omitting oxygen. The Ir–Ti oxide

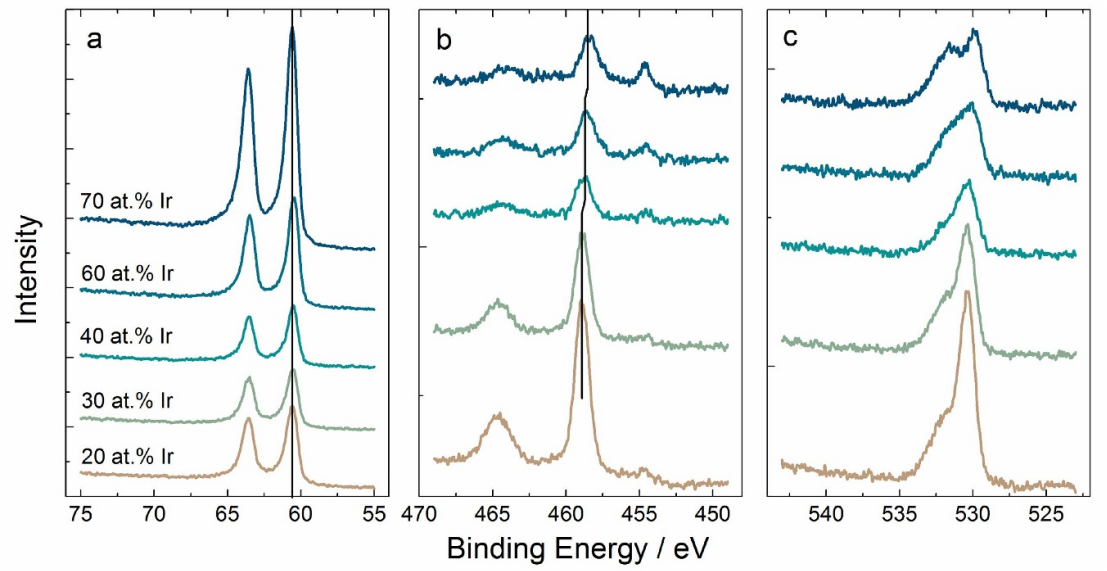

Figure 1. The XPS spectra of the Ir 4 f (a), Ti 2p (b) and O 1 s (c) levels for measurement areas with different Ir contents on thermally oxidized Ir–TiO_x material library. The binding energies of Ir $4f_{7/2}$ and Ti $2p_{3/2}$ peaks are shown in black lines in (a) and (b), respectively.

library was then used as the working electrode in the scanning flow cell (SFC)—inductively coupled plasma mass spectrometer (ICP-MS, NexION 350X, Perkin Elmer) based setup [33, 34]. The geometric surface area of the working electrode was defined by the size of the opening of the SFC (ca. $1 \cdot 10^{-2}$cm^2). All presented data are normalized to the geometric area of the working electrode. The inlet channel of the SFC contained a graphite rod, serving as the counter electrode. A commercial Ag/AgCl/3 M KCl electrode (Metrohm, Germany) was used as the reference electrode. The reversible hydrogen electrode (RHE) potential was measured in H_2-saturated electrolyte using a freshly prepared sputtered Pt thin film versus the saturated Ag/AgCl electrode. All potentials reported in the manuscript are presented versus the RHE scale. All electrochemical measurements were carried out in 0.1 M $HClO_4$ solution prepared by dilution of concentrated perchloric acid (Suprapur 96%, Merck, Germany) in ultrapure water (PureLabPlus system, Elga, 18 Mcm, TOC < 3 ppb). During measurements, the argon-saturated electrolyte was pumped with a constant flow rate of ca. 196 μl min^{-1} to the V-shaped channels of the SFC and further downstream to the ICP-MS. Downstream of the electrochemical cell and prior to introduction into the ICP-MS the electrolyte was mixed with an internal standard using a Y-connector (mixing ratio 1:1). As internal standards for detection of ^{55}Ti and ^{193}Ir isotopes, the isotopes of ^{50}Sc or ^{187}Re were used, respectively. The concentration of the internal standards in the solution was 10 μgl^{-1}. Calibration of the ICP-MS was performed on each experiment day prior to electrochemical measurements. The potentiostat (Gamry Reference 600, USA), electrolyte and gas flows as well as SFC components were automatically controlled using a homemade LabVIEW software. This enabled screening of the general behaviour of different locations on the material library under identical electrochemical protocols for direct comparison. Before the OER investigation the working electrode was always polarized at $E = 1.20$ V_{RHE} during 2 min for initial stabilization. Afterwards, the potential was swept from $E = 1.20$ V_{RHE} to a value corresponding to a current density of $j = 5$mA cm^{-2} with the scan rate of 10 mV s^{-1}. At least three measurements were done for each spot of the same composition to ensure the reproducibility of the results.

After this initial screening the long-term stability the most promising compositions that were synthesized as individual samples were tested in an H-cell with divided anodic and cathodic compartments. In a cell with such configuration the anodic and cathodic compartments were separated by a fine glass frit (Pine Research Instrumentation, USA). The volume of electrolyte in both compartments was adjusted to 10 ml and was kept constant during the measurements. A Pt foil placed in the cathodic compartment served as counter electrode. A saturated Ag/AgCl in the anodic compartment was used as a reference electrode.

The atom probe tomography (APT) experiments were conducted on a CAMECA LEAP 5000 XR instrument under laser pulsing mode at a specimen temperature of 60 K, with a target evaporation rate of 5 ions per 1000 pulses, a pulsing rate of 125 kHz, laser pulse energy of 60 pJ. The APT specimens were prepared by a site-specific lift-out procedure using a FEI Helios G4 CX focused ion beam (FIB)/scanning electron microscope. A 200-nm thick protective Cr-layer was coated on top of the sputtered thin film by

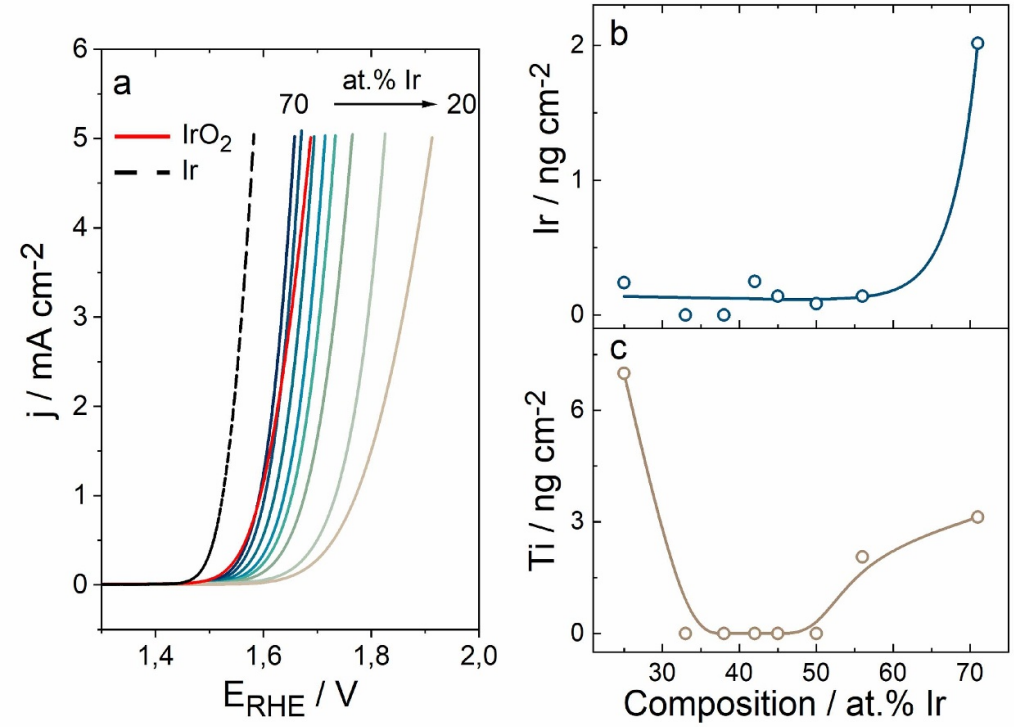

Figure 2. Summarized results on the activity-stability behavior of Ir–TiO_x material library. (a) Quasi steady-state anodic polarization curves for different Ir/Ti ratio of the material library in 0.1 M $HClO_4$ solution with a scan rate 10 mV s^{-1}. (b) Simultaneously measured amounts of dissolved Ir and (c) Ti. As the benchmarks, polarization curves obtained on sputtered metallic Ir and IrO_2 prepared by thermal oxidation of sputtered metallic film are shown by dashed black and red curves, respectively.

electron-beam deposition in order to protect the surface layers from FIB damage. The APT data were reconstructed and analysed using the commercial IVAS 3.8.4™ software.

3. Results

Characterization of Ir–TiO_x libraries by x-ray photoelectron spectrometry.

To ensure composition of the material library, XPS scans were recorded on as-deposited and thermally oxidized Ir–Ti composition gradient thin films. The atomic ratios between Ir and Ti remain the same after annealing at 350 °C for 4 h in air, which confirms an absence of significant segregation and diffusion of any of the elements within a thin surface layer during thermal treatment under these conditions. In all cases, iridium, titanium, oxygen and carbon were found on the surface. The spectra of Ir 4 f, Ti 2p and O 1 s recorded on the thermally oxidized gradient sample containing 20, 40, 60 and 70 at.% of Ir are shown in figure 1. For all samples, the Ir 4 f peak is observed at ca. 60.9 eV, indicating metallic state [35–38]. The symmetry of Ir 4 f peak was observed to be independent of the Ir–Ti ratio, suggesting that the main line in Ir 4 f level originates only from metallic Ir, or the amount of oxide species is below the detection limit. Regardless of the content of Ir in the samples its oxidation state remains constant. In the whole compositional range Ti 2p spectra have two resolved components. First, at lower binding energies (ca. 454.6 eV) one that corresponds to metallic Ti, while the second at higher binding energies can be assigned to Ti in oxides (ca 458.9 eV) [39]. The position of the peak corresponding to Ti^0 is found to be independent of Ti content in the films, while its contribution decreases with lower Ti concentration. The peak corresponding to Ti oxides shifts from 458.9 eV (TiO_2) to 458.4 eV as the content of Ir in the films increases from 20 to 70 at.%, most likely related to a decrease in oxygen stoichiometry of Ti oxides in Ir-enriched films. The O 1 s spectra presented in figure 1(c) exhibit presence of two resolved components corresponding to O in the oxide lattice (at lower binding energies) and O from OH groups and water molecules on the electrode surface (at higher binding energies). With increasing content of Ir in the films the O 1 s peak shifts from 530.4 eV to 529.8 eV. The contribution of OH and H_2O is also increasing. The observed variation can originate from the difference in the oxygen affinity for Ir and Ti. After the application of the electrochemical protocol no change in spectra of these elements was observed (figure S4), which indirectly suggests high stability of these materials.

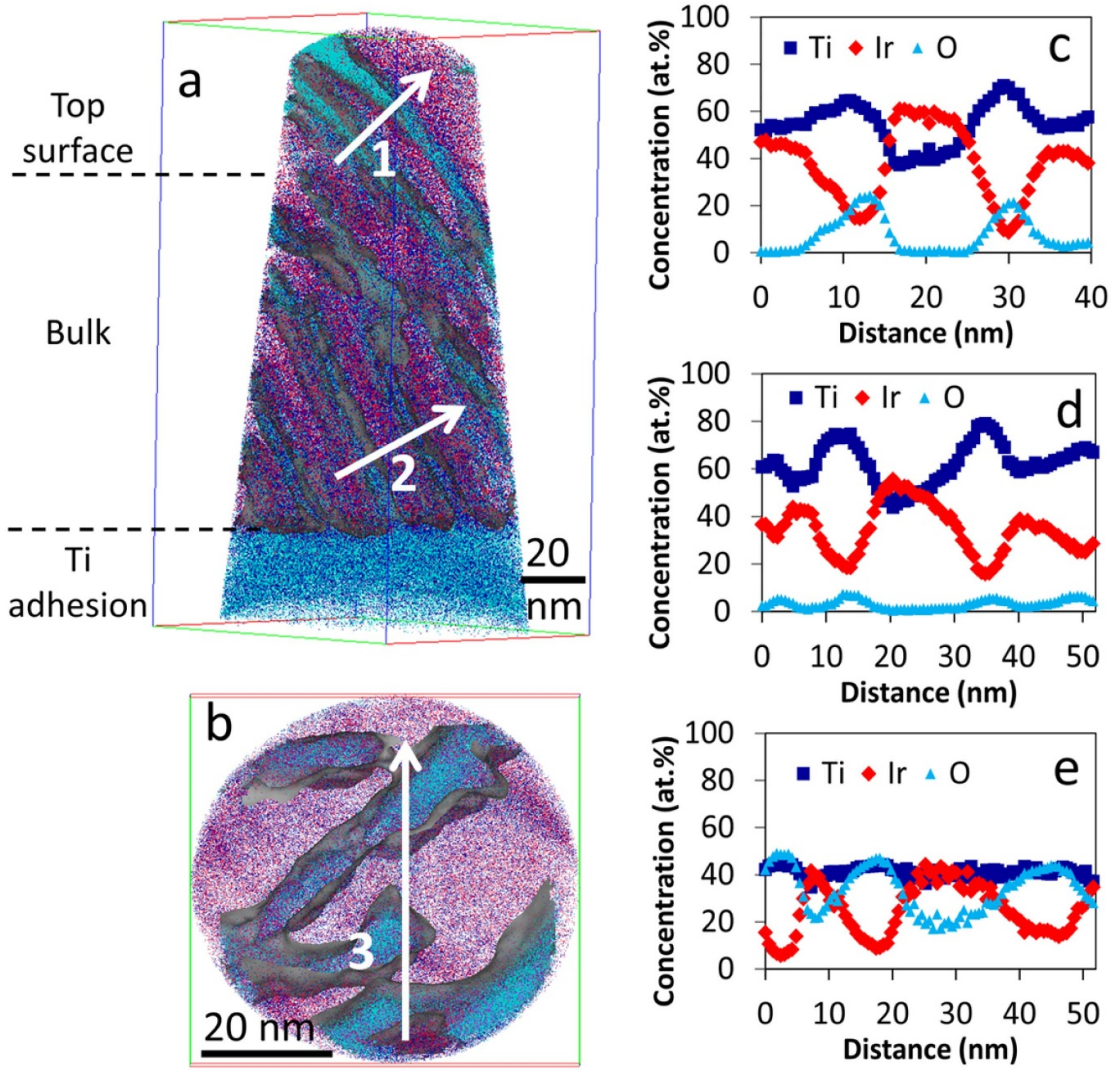

Figure 3. APT data on Ir–TiO_x containing 50 at.% of Ir. (a) Side view of APT reconstruction of the as-deposited sample. (b) Top-down view of APT reconstruction. (c), (d) and (e), One-dimensional composition profiles from the regions along the arrows labelled 1, 2 and 3 in (a) and (b). The grey areas show Ti-enriched regions, with the content of Ti in the range of 50–80 at.%. The Cr protective layer is not shown in the reconstruction.

Screening of Ir–TiO_x material library for desired electrocatalytic properties.

Figure 2(a) shows anodic polarization curves recorded on the Ir–TiO_x material library. For straightforward comparison with other materials examined by SFC-ICP-MS in the past, the value of potential at a current density of 5 mA cm^{-2} is chosen as a criterion of reactivity of these catalysts. In addition, the polarization curves for thermally prepared IrO_2 and metallic Ir are presented for benchmarking. The benchmark Ir electrode was synthesized using magnetron sputtering under conditions similar to those for Ir–Ti mixtures, while IrO_2 was prepared by annealing of such film in air at 600 C during 5 h to ensure formation of rutile phase [13]. Note, that in line with literature data [31] materials containing less than 20 at.% of Ir have poor conductivity and are not considered here. All of the investigated Ir–TiO_x mixtures show lower reactivity than metallic Ir, yet the materials with an Ir content of more than 50 at.% exhibit reactivity comparable to thermally grown IrO_2. With decreasing Ir content in the material library, the potential at 5 mA cm^{-2} shifts to higher anodic values, i.e. the activity of the catalysts for the OER decreases.

The dissolution of Ir and Ti is measured simultaneously with the anodic potential sweep (LSV). Figures 2(b) and (c) summarize the integrated amounts of dissolved Ir and Ti during one LSV as a function of electrode composition. One can see that the rate of Ir dissolution in this short experiment remains negligible as long as its fraction in the electrode does not exceed 60 at.%. The loss of Ir from a sample containing 70 at.% of Ir was about 2 ng cm^{-2}. For comparison, under the same electrochemical conditions about 0.2 ng cm^{-2} of Ir is dissolved from thermally prepared IrO_2, while a metallic electrode loses about 10 ng cm^{-2} of Ir (see dissolution profiles in figure S5). The dissolution of Ti is below the detection limit in the range of 30–50 at.% of Ir, while it increases both at lower and higher Ir compositions. During the anodic

potential sweep more than 7 ng cm^{-2} Ti is removed from the electrodes containing less than 20 at.% of Ir, while at high Ir contents around 3 ng cm^{-2} of Ti is lost. Considering that materials containing between 30 and 50 at.% of Ir show the best electrocatalytic performance, we further investigate the performance under long-term polarization of a representative sample within this composition range. Moreover, as the nonlinearity of the dissolution behaviour in this compositional range cannot be explained based on the XPS data only, the atomic scale structure of the 50 at.% of Ir sample is also considered in more detail.

Atomic scale insights into the composition of Ir–TiO_x with 50 at.% of Ir.

The atomic scale structure of an Ir–TiO_x electrode with 50 at.% of Ir was revealed by APT. APT provides information on the elemental distribution in three dimensions [40–42]. Figures 3(a) and (b) show the side and top-down views of the 3D APT reconstruction of a catalyst film, respectively. The profiles in figures (c)–(e) show the compositional variations in a near surface layer, bulk, and lateral surface. Based on the APT data the volume of the catalyst can be described as a composite alloy containing matrix with the nominal composition of 40 at.% of Ir decorated with Ti enriched regions. The content of Ti in such clusters ranges from 70 to 80 at.%. The average composition roughly corresponds to 50 at.% of Ir, in line with EDX and XPS data. The composition profiles of the near surface region are shown in figures 3(c) and (e). The data suggests that the thermal oxidation occurs in the near surface regions and only Ti-enriched clusters are prone to oxidize. The composition of the oxide clusters in the near surface region corresponds to 70 at.% of Ti, 25 at.% of O and 5 at.% of Ir. The oxygen content tends to decrease with the depth. The composition of the metallic matrix in the top surface region increases to 50 at.% Ir as was also revealed by XPS (figure 3(c)). Distribution of oxygen is inhomogeneous in all directions.

Long-term performance of the Ir–TiO_x anode containing 50 at.% of Ir.

The SFC-ICP-MS measurements for gas evolving reactions are typically limited due to possible blocking of the working electrode by bubble formation over time, which is why they can only provide a first information on the initial dissolution rates. In order to examine the long-term stability of anode materials, galvanostatic measurements are performed in an H-cell with divided anodic and cathodic compartments. In these experiments samples of the electrolyte are taken periodically from both compartments for analysis of metal content using off-line ICP-MS. During the entire experiment no Ir nor Ti was detected in the cathodic compartment. In the anodic compartment only after 120 min significant metal dissolution could be found (figure 4). The Ti concentration remains constant below 1 ng cm^{-2} after ca. 120 min, while it takes about 200 min for the Ir concentration to stabilize at around 8 ng cm^{-2}. Note that this equilibrium might be special for the given H-cell and the volume of electrolyte, and surely differs from the behaviour of flow reactors where due to the constant purging such an equilibrium might not be reached. For straightforward comparison of evolution of the electrocatalytic activity of the electrode the quasi steady state polarization curve was taken after the H-cell experiments (curve 2 in figure S6). In these conditions to achieve current density of 5 mA cm^{-2} additional 25 mV are required, which indicates slight drop of activity.

4. Discussion

Catalyst materials prepared by dispersing the noble metals in a more stable nonprecious matrix have been intensively investigated. Among others, TiO_2-containing mixtures were successfully employed in dimensionally stable anodes for chlorine evolution [10, 43]. For OER related applications the main research efforts were focused on reduction of the amount of the noble metal in the electrode without a significant decrease in electronic conductivity and reactivity [9]. As was shown in literature [31], the reduction of the Ir content in Ir/TiO_x results in drastic changes in electrical conductivity and the respective OER performance as a catalyst. Anodes containing various mixtures of Ti, Ir and Sn were shown to have improved stability, though the activity was lower than metallic Ir and also what thermally annealed IrO_2 could provide [44]. Here, the screening of the Ir–TiO_x materials library (figure 2) shows that the activity of such mixtures can be comparable to IrO_2. The XPS data in figure 1 confirms the initial metallic state of Ir in the whole compositional range that leads to the high reactivity, when the sample only experiences a moderate thermal treatment of short duration. Apparently, the oxidation of Ir is hindered during short-term treatment in air at rather mild temperatures. It was previously reported that the heat-treatment at temperatures below 400 C is not sufficient to form rutile IrO_2 [45–47]. Considering the high affinity of Ti for oxygen, its presence in the electrodes makes oxidation of Ir relatively even more unfavorable. The oxidation of Ti is also incomplete independent of the composition, which could be explained by either the low partial pressure of oxygen in air, as well as the low temperature and duration of the annealing treatment or limited diffusion of oxygen into the film. This results in sufficiently high conductivity. In line with previous reports [48], the reactivity decreases with increasing content of Ti in the electrode (figure 2(a)). This can be explained by both the decrease in the number of electrochemically active sites provided exclusively by Ir and the increasing contribution of less conductive oxides of Ti (figure 2(b)). The observed trend supports previously published

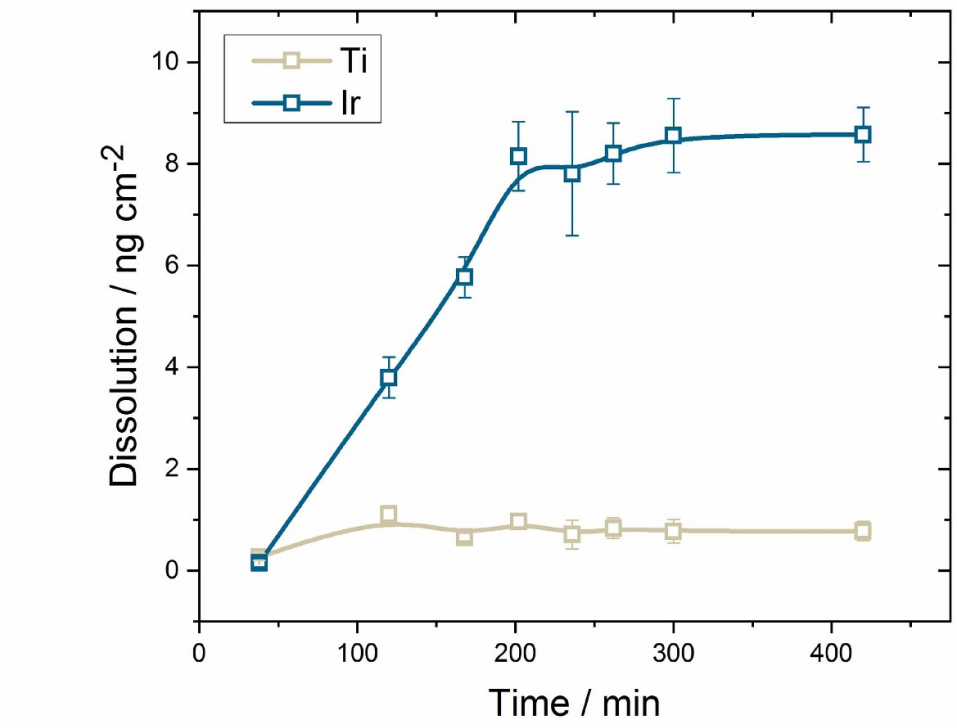

Figure 4. Dependence of the amount of dissolved Ir and Ti from an Ir–TiO_x anode containing 50 at.% Ir on electrolysis duration. The anodic polarization was performed in an H-cell with divided anodic and cathodic compartment at 1 mA cm^{-2} in 0.1 M $HClO_4$.

statements on the overall deterioration in OER activity at high Ti contents in binary noble metals-based mixed oxides, including those containing Ir [31, 48, 49].

Stability data demonstrates the increase in Ir dissolution with its increasing content in the electrode (figure 2(b)). A higher Ir loading on the surface of the electrode results in an increased number of active sites available for the OER and improved activity. Considering our previous reports suggesting that Ir dissolution is triggered by the OER itself [16, 17, 50], the amount of dissolved Ir should increase with increasing activity. A similar dissolution behaviour was previously reported for Ir–Ru mixed oxides [51]. However, in contrast to the Ir–Ru system where both components show increased dissolution with their increasing content, the dependence of Ti dissolution from Ir–TiO_x anodes on the electrode composition is more complex (figure 2(c)). In particular, the Ti dissolution rate increases at both high and low loadings of Ti in the films, while at the mid-composition range the dissolution is below the detection limit in SFC-ICP-MS experiments. Apparently, the dissolution of Ti results from the metallic phase present in the films, as shown by XPS data in figure 1(b). Under OER conditions this metallic phase converts into an oxide, which is accompanied by dissolution, as was reported previously [41]. According to the XPS data in figure 1(c) the content of metallic Ti phase increases for materials with high Ir loadings and so does the dissolution. In contrast, a high dissolution rate of Ti at low Ir contents can be explained by the significant drop in the activity, leading to more positive anodic potential at the current density of 5 mA cm^{-2}. Interestingly, mixtures containing ca 30–50 at.% of Ir exhibit an extraordinary immunity towards dissolution of both components, which results from the formation of Ti-enriched oxide regions with superior stability as revealed by APT (figure 3). The overall non-linear activity-stability relationship in such materials originates from the coexistence of highly reactive metallic Ir and a stable phase of titanium oxides. The catalytic properties of materials containing a Ti oxide phase tend to suffer from their semiconducting or even insulating nature. However, for the 50% sample investigated in more detail here the APT data (figure 3) reveals that the titanium oxide phase contains with at least 5 at.% of Ir, which boosts the conductivity of the catalytic layer.

In order to compare the stability behaviour of Ir–TiO_x to other thin film catalysts we estimated their stability numbers (S-number) in conditions of quasi-steady state anodic polarization at 1 mA cm^{-2} based on the data in figure 4. The S-number is a universal metric independent of the surface area and catalyst loading

Table 1. The S-number calculated for different Ir-containing catalysts.

Anode material	S-number[a]	Conditions	Reference
$Ir_{0.5}Ti_{0.5}O_x$	$1.5 \cdot 10^6$	0.1 M $HClO_4$; steady-state, 1 mA cm^{-2}	This work
$Ir_{0.7}Sn_{0.3}O_x$	$1.6 \cdot 10^5$	0.1 M $HClO_4$; steady-state, 1 mA cm^{-2}	[23, 52]
	$5 \cdot 10^4$	0.1 M $HClO_4$; 5 min, 1 mA cm^{-2}	
$Ir_{0.7}Ru_{0.3}O_2$[b]	$1.0 \cdot 10^6$ (Ir)[c] $1.0 \cdot 10^5$ (Ru)	0.1 M $HClO_4$; 1 min, 1 mA cm^{-2}	[51, 52]
IrO_2	$9.2 \cdot 10^5$	0.1 M $HClO_4$; 10 min, 1 mA cm^{-2}	[50]
IrO_x-amorphous	$5.0 \cdot 10^4$	0.1 M $HClO_4$; 5 min, 1 mA cm^{-2}	[50]
Ir metal	$1.0 \cdot 10^5$	0.1 M $HClO_4$; 5 min, 1 mA cm^{-2}	[50]
$SrIrO_3$, thin film	$8.0 \cdot 10^4$	0.1 M $HClO_4$; 10 min, 1 mA cm^{-2}	[50]
IrO_2@TiO_2 NPs	$1.0 \cdot 10^4$	0.1 M $HClO_4$; 5 min, 100 mA mg^{-1}	[26]

[a] For alloys and mixed oxides, the S-number should be considered for all elements reactive towards the OER

[b] Here, dissolution of both Ir and Ru was normalized by the total amount of formed oxygen molecules, since the number of oxygen molecules evolved on each type of active sites remains unknown

[c] In $Ir_{0.7}Ru_{0.3}O_2$ anode the OER mainly takes place on the more reactive Ru active sites, which explains the high stability number for Ir. However, dissolution of both elements should be considered for the overall stability.

(in case of nanoparticles), and corresponds to the number of oxygen molecules evolved versus the amount of dissolved catalytically active atoms (herein Ir) [50]. Considering the summarized data shown in table 1, all OER catalysts exhibit S-numbers comparable to that of amorphous IrO_x. Although the Ir–Ru mixed oxide also shows a relatively high S-number for Ir, it should be considered that in this case the OER occurs mainly on Ru active sites, resulting in intense Ru corrosion, while Ir contributes to the reaction to a lesser extent. The Ir–TiO_x anode exhibits high stability with an S-number comparable to that reported for thermally grown IrO_2, exceeding previously reported performance of IrO_2@TiO_2 nanoparticles [26]. Even though a direct comparison of thin film materials with nanoparticles is rather complicated, the observed difference in durability estimation suggests that formation of the mixed oxide phase of Ir and Ti is crucial for the stability of the catalyst and requires further investigation and optimization.

Although long-term durability of Ir–Ti mixtures has still to be proven, the addition of Ti oxide to Ir seems to be a promising way to achieve the balance between activity and stability and decrease the Ir loading. Important to note is, however, that the stability of Ir in such systems can suffer from conductivity issues leading to potential shifts and further dissolution. Thorough analysis of the electronic properties of Ir–Ti mixtures has to be considered for the design of superior catalysts. A comprehensive study of the relationship between electronic properties and activity/stability for such mixed oxide anodes in acidic media will be a topic of a future work.

5. Conclusions

Stability and activity towards the OER of a model Ir–Ti mixed oxide materials library over a wide composition range were examined using the SFC-ICP-MS set-up. The results concerning the dissolution of Ir and Ti show that independent of the Ir content in the electrode, the rate of its dissolution is observed to be lower than that of thermally prepared IrO_2, while catalysts containing at least 50 at.% of Ir exhibit relatively high activity. This beneficial balance between activity and stability originates from the atomic-scale structure of this catalyst in which metallic Ir, providing high activity, coexists with Ti-enriched oxide phases, which ensure stability towards dissolution. Overall, our data show that Ir–Ti mixtures can be promising OER catalysts with both high activity and stability against dissolution.

Acknowledgments

O K acknowledges financial support from the Helmholtz Networking and Initiative Fund. T L thanks Zentrum für Grenzflächendominierte Höchstleistungswerkstoffe (ZGH) at Ruhr University Bochum for the access of infrastructure (FEI Helios G4 CX FIB/SEM and Cameca LEAP 5000 XR).

ORCID iD

Olga Kasian https://orcid.org/0000-0001-6315-0637

References

[1] Barbir F 2005 PEM electrolysis for production of hydrogen from renewable energy sources *Sol. Energy* **78** 661–9
[2] Rossmeisl J, Qu Z W, Zhu H, Kroes G J and Nørskov J K 2007 Electrolysis of water on oxide surfaces *J. Electroanal. Chem.* **607** 83–9
[3] Trasatti S 1995 Electrochemistry and environment: the role of electrocatalysis *Int. J. Hydrog. Energy* **20** 835–44
[4] Carmo M, Fritz D L, Mergel J and Stolten D 2013 A comprehensive review on PEM water electrolysis *Int. J. Hydrogen Energy* **38** 4901–34
[5] Danilovic N, Ayers K E, Capuano C, Renner J N, Wiles L and Pertoso M 2016 (Plenary) Challenges in going from laboratory to megawatt scale PEM electrolysis *ECS Trans.* **75** 395–402
[6] Binninger T, Mohamed R, Waltar K, Fabbri E, Levecque P, Kotz R and Schmidt T J 2015 Thermodynamic explanation of the universal correlation between oxygen evolution activity and corrosion of oxide catalysts *Sci. Rep.* **5** 12167
[7] Danilovic N *et al* 2014 Activity–stability trends for the oxygen evolution reaction on monometallic oxides in acidic environments *J. Phys. Chem. Lett.* **5** 2474–8
[8] Hodnik N, Jovanovič P, Pavlišič A, Jozinović B, Zorko M, Bele M, Šelih V S, Šala M, Hočevar S and Gaberšček M 2015 New insights into corrosion of ruthenium and ruthenium oxide nanoparticles in acidic media *J. Phys. Chem.* C **119** 10140–7
[9] Trasatti S 1984 Electrocatalysis in the anodic evolution of oxygen and chlorine *Electrochim. Acta* **29** 1503–12
[10] Trasatti S 2000 Electrocatalysis: understanding the success of DSA® *Electrochim. Acta* **45** 2377–85
[11] Schalenbach M, Tjarks G, Carmo M, Lueke W, Mueller M and Stolten D 2016 Acidic or alkaline? Towards a new perspective on the efficiency of water electrolysis *J. Electrochem. Soc.* **163** F3197–208
[12] Siracusano S, Hodnik N, Jovanovic P, Ruiz-Zepeda F, Šala M, Baglio V and Aricò A S 2017 New insights into the stability of a high performance nanostructured catalyst for sustainable water electrolysis *Nano Energy* **40** 618–32
[13] Cherevko S *et al* 2016 Oxygen and hydrogen evolution reactions on Ru, RuO2, Ir, and IrO2 thin film electrodes in acidic and alkaline electrolytes: A comparative study on activity and stability *Catal. Today* **262** 170–80
[14] Cherevko S, Zeradjanin A R, Topalov A A, Kulyk N, Katsounaros I and Mayrhofer K J J 2014 Dissolution of noble metals during oxygen evolution in acidic media *ChemCatChem* **6** 2219–23
[15] Jovanovič P *et al* 2017 Electrochemical dissolution of iridium and iridium oxide particles in acidic media: transmission electron microscopy, electrochemical flow cell coupled to inductively coupled plasma mass spectrometry and x-ray absorption spectros-copy study *J. Am. Chem. Soc.* **139** 12837–46
[16] Kasian O, Grote J-P, Geiger S, Cherevko S and Mayrhofer K J J 2018 The common intermediates of oxygen evolution and dissolution reactions during water electrolysis on iridium *Angew. Chem., Int. Ed. Engl.* **57** 2488–91
[17] Kasian O *et al* 2019 Degradation of iridium oxides via oxygen evolution from the lattice: correlating atomic scale structure with reaction mechanisms *Energy Environ. Sci.* **12** 3548–55
[18] Choe S, Lee B-S, Cho M K, Kim H-J, Henkensmeier D, Yoo S J, Kim J Y, Lee S Y, Park H S and Jang J H 2018 Electrodeposited IrO2/Ti electrodes as durable and cost-effective anodes in high-temperature polymer-membrane-electrolyte water electrolyzers *Appl. Catal.* B **226** 289–94
[19] Kamegaya Y, Sasaki K, Oguri M, Asaki T, Kobayashi H and Mitamura T 1995 Improved durability of iridium oxide coated titanium anode with interlayers for oxygen evolution at high current densities *Electrochim. Acta* **40** 889–95
[20] Li G, Li K, Yang L, Chang J, Ma R, Wu Z, Ge J, Liu C and Xing W 2018 Boosted performance of Ir species by employing TiN as the support toward oxygen evolution reaction *ACS Appl. Mater. Interfaces* **10** 38117–24
[21] Bernt M and Gasteiger H A 2016 Influence of ionomer content in IrO2/TiO2 electrodes on PEM water electrolyzer performance *J. Electrochem. Soc.* **163** F3179–89
[22] Lončar A, Moriau L, Stojanovski K, Ruiz-Zepeda F, Jovanovic P, Bele M, Gaberscek M and Hodnik N 2020 Ir/TiONx/C high-performance oxygen evolution reaction nanocomposite electrocatalysts in acidic media: synthesis, characterization and electrochemical benchmarking protocol *J. Phys. Energy* **2** 02LT01
[23] Kasian O, Geiger S, Schalenbach M, Mingers A M, Savan A, Ludwig A, Cherevko S and Mayrhofer K J J 2018 Using instability of a non-stoichiometric mixed oxide oxygen evolution catalyst as a tool to improve its electrocatalytic performance *Electrocatalysis* **9** 139–45
[24] Li G, Yu H, Yang D, Chi J, Wang X, Sun S, Shao Z and Yi B 2016 Iridium-Tin oxide solid-solution nanocatalysts with enhanced activity and stability for oxygen evolution *J. Power Sources* **325** 15–24
[25] Liu G, Xu J, Wang Y and Wang X 2015 An oxygen evolution catalyst on an antimony doped tin oxide nanowire structured support for proton exchange membrane liquid water electrolysis *J. Mater. Chem.* A **3** 20791–800
[26] Pham C V, Bühler M, Knöppel J, Bierling M, Seeberger D, Escalera-López D, Mayrhofer K J J, Cherevko S and Thiele S 2020 IrO2 coated TiO2 core-shell microparticles advance performance of low loading proton exchange membrane water electrolyzers *Appl. Catal.* B **269** 118762
[27] Mazúr P, Polonský J, Paidar M and Bouzek K 2012 Non-conductive TiO2 as the anode catalyst support for PEM water electrolysis *Int. J. Hydrog. Energy* **37** 12081–8
[28] Lv H, Zhang G, Hao C, Mi C, Zhou W, Yang D, Li B and Zhang C 2017 Activity of IrO2 supported on tantalum-doped TiO2 electrocatalyst for solid polymer electrolyte water electrolyzer *RSC Adv.* **7** 40427–36
[29] Oh H-S, Nong H N, Teschner D, Reier T, Bergmann A, Gliech M, Ferreira de Araújo J, Willinger E, Schloegl R and Strasser P 2016 Electrochemical catalyst-support effects and their stabilizing role for IrOx nanoparticle catalysts during the oxygen evolution reaction (OER) *J. Am. Chem. Soc.* **138** 12552–63
[30] Saveleva V A *et al* 2020 Insight into the mechanisms of high activity and stability of iridium supported on antimony-doped tin oxide aerogel for anodes of proton exchange membrane water electrolyzers *ACS Catal.* **10** 2508–16
[31] Bernsmeier D, Bernicke M, Schmack R, Sachse R, Paul B, Bergmann A, Strasser P, Ortel E and Kraehnert R 2018 Oxygen evolution catalysts based on Ir–Ti mixed oxides with templated mesopore structure: impact of Ir on activity and conductivity *ChemSusChem* **11** 2367–74
[32] Oakton E, Lebedev D, Povia M, Abbott D F, Fabbri E, Fedorov A, Nachtegaal M, Copéret C and Schmidt T J 2017 IrO2-TiO2: a high-surface-area, active, and stable electrocatalyst for the oxygen evolution reaction *ACS Catal.* **7** 2346–52
[33] Schuppert A K, Topalov A A, Savan A, Ludwig A and Mayrhofer K J J 2014 Composition-dependent oxygen reduction activity and stability of Pt-Cu thin films *ChemElectroChem* **1** 358–61
[34] Topalov A A, Katsounaros I, Auinger M, Cherevko S, Meier J C, Klemm S O and Mayrhofer K J J 2012 Dissolution of Platinum: limits for the Deployment of Electrochemical Energy Conversion? *Angew. Chem., Int. Ed. Engl.* **51** 12613–5

[35] Augustynski J, Koudelka M, Sanchez J and Conway B E 1984 ESCA study of the state of iridium and oxygen in electrochemically and thermally formed iridium oxide films *J. Electroanal. Chem. Interfacial Electrochem.* **160** 233–48
[36] Massué C, Pfeifer V, Van gastel M, Noack J, Algara-Siller G, Cap S and Schlögl R 2017 Reactive electrophilic OI− species evidenced in high-performance iridium oxohydroxide water oxidation electrocatalysts *ChemSusChem* **10** 4786–98
[37] Pfeifer V *et al* 2016 The electronic structure of iridium and its oxides *Surf. Interface Anal.* **48** 261–73
[38] Pfeifer V *et al* 2016 The electronic structure of iridium oxide electrodes active in water splitting *Phys. Chem. Chem. Phys.* **18** 2292–6
[39] da Silva L A, Alves V A, de Castro S C and Boodts J F C 2000 XPS study of the state of iridium, platinum, titanium and oxygen in thermally formed IrO 2 +TiO 2 +PtO X films *Colloids Surf.* A **170** 119–26
[40] Lim J, Kim S-H, Aymerich Armengol R, Kasian O, Choi -P-P, Stephenson L T, Gault B and Scheu C 2020 Atomic-scale mapping of impurities in partially reduced hollow TiO2 nanowires *Angew. Chem., Int. Ed. Engl.* **59** 5651–5
[41] Schweinar K, Gault B, Mouton I and Kasian O 2020 Lattice oxygen exchange in rutile IrO2 during the oxygen evolution reaction *J. Phys. Chem. Lett.* **11** 5008–14
[42] Schweinar K, Nicholls R L, Rajamathi C R, Zeller P, Amati M, Gregoratti L, Raabe D, Greiner M, Gault B and Kasian O 2020 Probing catalytic surfaces by correlative scanning photoemission electron microscopy and atom probe tomography *J. Mater. Chem.* A **8** 388–400
[43] Gorodetskii V V, Neburchilov V A and Alyab'eva V I 2005 Titanium anodes with an active coating based on iridium oxides.pdf *Russ. J. Electrochem.* **41** 1111–7
[44] Antolini E 2014 Iridium as catalyst and cocatalyst for oxygen evolution/reduction in acidic polymer electrolyte membrane electrolyzers and fuel cells *ACS Catal.* **4** 1426–40
[45] Geiger S, Kasian O, Shrestha B R, Mingers A M, Mayrhofer K J J and Cherevko S 2016 Activity and stability of electrochemically and thermally treated iridium for the oxygen evolution reaction *J. Electrochem. Soc.* **163** F3132–38
[46] Gorodetskii V V and Neburchilov V A 2007 Tantalum oxide effect on the surface structure and morphology of the IrO2 and IrO2 + RuO2 + TiO2 coatings and on the corrosion and electrochemical properties of anodes prepared from these *Russ. J. Electrochem.* **43** 223–8
[47] Cherevko S, Reier T, Zeradjanin A R, Pawolek Z, Strasser P and Mayrhofer K J J 2014 Stability of nanostructured iridium oxide electrocatalysts during oxygen evolution reaction in acidic environment *Electrochem Commun.* **48** 81–85
[48] Endo K, Katayama Y, Miura T and Kishi T 2002 Composition dependence of the oxygen-evolution reaction rate on Ir x Ti1− x O2 mixed-oxide electrodes *J. Appl. Electrochem.* **32** 173–8
[49] Kasian O I, Luk'yanenko T V and Velichenko A B 2013 Electrochemical properties of heat-treated platinized titanium *Prot. Met. Phys. Chem. Surf.* **49** 559–66
[50] Geiger S *et al* 2018 The stability number as a metric for electrocatalyst stability benchmarking *Nat. Catal.* **1** 508–15
[51] Kasian O, Geiger S, Stock P, Polymeros G, Breitbach B, Savan A, Ludwig A, Cherevko S and Mayrhofer K J J 2016 On the origin of the improved ruthenium stability in RuO2–IrO2 mixed oxides *J. Electrochem. Soc.* **163** F3099–104
[52] Kasian O, Geiger S, Mayrhofer K J J and Cherevko S 2019 Electrochemical on-line ICP-MS in electrocatalysis research *Chem. Rec.* **19** 2130–42